Quantum Phase Recognition using Quantum Tensor Networks

Shweta Sahoo,[*] Utkarsh Azad,[†] and Harjinder Singh
Center for Computational Natural Sciences and Bioinformatics,
International Institute of Information Technology, Hyderabad.
Center for Quantum Science and Technology,
International Institute of Information Technology, Hyderabad.
(Dated: August 12, 2022)

Machine learning (ML) has recently facilitated many advances in solving problems related to many-body physical systems. Given the intrinsic quantum nature of these problems, it is natural to speculate that quantum-enhanced machine learning will enable us to unveil even greater details than we currently have. With this motivation, this paper examines a quantum machine learning approach based on shallow variational ansatz inspired by tensor networks for supervised learning tasks. In particular, we first look at a classical image classification task using the Fashion-MNIST dataset and study the effect of repeating tensor network layers on ansatz's expressibility and performance. Finally, we use this strategy to tackle the problem of quantum phase recognition for the Transverse Ising and Heisenberg spin models in one and two dimensions, where we were able to reach $\geq 98\%$ test-set accuracies with both multi-scale entanglement renormalization ansatz (MERA) and tree tensor network (TTN) inspired parametrized quantum circuits.

Keywords: Quantum Computing, Quantum Machine Learning, Quantum Many-body Systems, Quantum-Classical Algorithms

I. Introduction

Machine learning (ML) offers tools and techniques to learn and predict patterns that emerge in data. One crucial avenue of this pattern recognition task is classification, which involves predicting class labels for the input data and has found applications in speech recognition [1], biometric identification [2], object classification [3], disease identification [4] and many more. These applications result from immense leaps classical ML algorithms have made in dealing with various challenging datasets. Lately, based on these successes, ML algorithms have been used for problems related to many-body physical systems, such as recognizing phases of matter [5, 6]. Even though they have shown more promising results for studying relevant and useful many-body systems than the best contemporary classical algorithms, they still do not alleviate the sign problem [7], which usually emerges in such calculations and causes an exponential slowdown.

More recently, there has been an ongoing effort to develop quantum-enhanced machine learning algorithms that leverage quantum computers to tackle traditional ML problems [8]. These algorithms are typically based on a class of hybrid quantum-classical algorithms called variational quantum algorithms (VQAs), such as variational quantum eigensolver (VQE) [9] and variational quantum linear solvers (VQLS) [10] that have been used to find the ground state of a Hamiltonian and solve systems of linear equations on noisy intermediate-scale quantum (NISQ) hardware [11]. The relatively short depth of the parameterized quantum circuits (PQCs) used in these algorithms makes them an ideal candidate for achieving good results on NISQ devices without error correction codes. [12].

In principle, although PQCs are analogous to classical neural networks structurally, they can exploit additional computational resources due to the presence of quantum mechanical phenomena such as superposition and entanglement [13]. The basic working principle of VQAs is to optimize the parameters of PQC, also referred to as an *ansatz*, using a classical optimization routine to minimize a cost function defined on measurements taken on the qubits present in the ansatz. Therefore, the performance of these algorithms is majorly based on the structure of the ansatz [14]. Hence, it is crucial to analyze and have some basic insights into the ansatz for a particular problem or application to assess and improve their trainability.

In this paper, we use a VQE-based algorithm to classify classical and quantum data. For the former, we look at the task of classification of Fashion MNIST dataset [15], whereas, for the latter, we tackle the problem of classification of the quantum phase of 1-D and 2-D transverse Ising and XXZ Heisenberg spin system. We employ multi-scale entanglement renormalization ansatz (MERA) and tree tensor network (TTN) states for building the ansatz for the variational routine. Finally, we also use expressibility and entangling capability analysis for choosing the structure of unitary block for these ansätze (Figs. 2a and 2b) that helps us make use of shorter-depth blocks than the general $SU(4)$ one suggested in [16].

Structure : In section II, we start off with a background on quantum tensor networks and spin systems, followed by a description of the experiments and their corresponding results conducted by us in section III. Lastly, in section IV, we provide our conclusions and discussions on our results and future work.

* shweta.sahoo@research.iiit.ac.in
† utkarsh.azad@research.iiit.ac.in

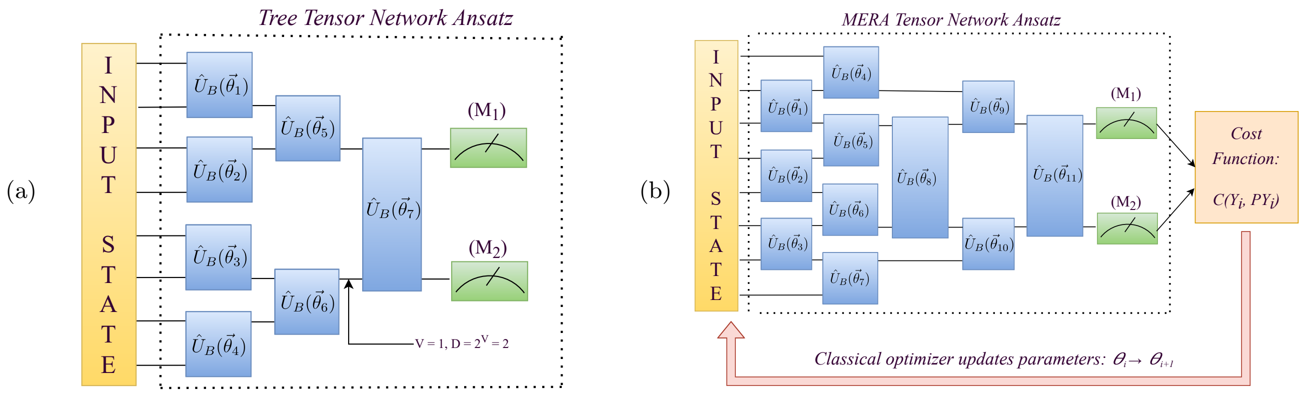

FIG. 1: **Tensor network inspired variational ansätze**: (a) Structure of the tree tensor network (TTN) ansatz with bond dimension two, and (b) variational workflow using multi-scale entanglement renormalization ansatz (MERA) tensor network.

II. Background

A. Quantum Tensor Networks

Tensor networks are essentially approximations of very large tensors using smaller, easier to handle tensors [17]. Tensor networks like the matrix product state (MPS) [18], tree tensor networks (TTN) [19] and multi-scale entanglement renormalization ansatz (MERA) [20] can be constructed using a quantum circuit [21, 22].

Recently, the use of quantum circuits based on tensor networks have been explored in the domain of machine learning for both generative [23] and discriminative tasks [16, 21, 24]. The bond dimension of a tensor network is the dimension of the index connecting smaller tensors together. The bond dimension, D, of a tensor network that has been realized using a quantum circuit is 2^v, where v qubits connect different subtrees. The main motivation behind using tensor network inspired quantum circuits is the increase in expressibility of the ansatz with increasing bond dimension to the point that for a sufficiently huge bond dimension, the entire state space can be covered. In the classical scenario, such systems will be too computationally expensive to deal with [21]. Moreover, it is highly likely that in the case of quantum data such as the wavefunction of a system, usage of classical methods will be intractable due to the exponential increase of information that needs to be encoded and computed with the increase in particles.

Circuits with a hierarchical structure like that of a MERA or TTN tensor network have been used in the classification of images like those in the MNIST dataset [16, 24]. A hybrid classical-quantum MPS-VQC has been used in image classification tasks with the MPS being the feature extractor for the images. While the MPS tensor network in this case is classical in nature, it can be replaced with an equivalent quantum circuit paving the way for the usage of quantum tensor networks as feature extractors [25]. Various tensor network ansätze have also been used for Quantum phase recognition tasks for the 1-D Heisenberg [16] and Transverse Ising models [26] with good results.

B. Spin Systems

The study of spin systems is important in order to understand the magnetic properties of a system at a macroscopic level. This is because the magnetic moment of an atom has contributions from the electron spins. The alignment of many such spins on a macroscopic scale defines the magnetic properties of the system. This alignment of spins is driven by the exchange interaction between the atoms. Exchange interaction is a short range, powerful interaction that occurs due to the electrical forces between electrons in the atoms [27, 28]. In this paper we will deal with spin systems where the atomic dipoles are depicted by points on a 1-D and 2-D square lattice. The exchange interaction between atoms is limited to nearest neighbors and is given by the general formula:

$$\varepsilon = \alpha \boldsymbol{S_1}.\boldsymbol{S_2} + \beta S_1^Z S_2^Z$$

S_1 and S_2 are the spins of the two neighboring atoms in question. We will be considering variants of the special case of $\alpha = 0$ and $\beta = J$ which is the Ising model of interaction and $\alpha = J$ and $\beta = 0$ which is the Heisenberg model of interaction [27]. Spin systems undergo quantum phase transitions. A quantum phase transition is a point of non-analyticity in the energy graph of the ground state of the Hamiltonian of the system caused due to quantum fluctuations at 0 K [29]. Since many complex models can be approximated as spin systems, quantum phase recognition allows us to derive and understand the properties of such systems.

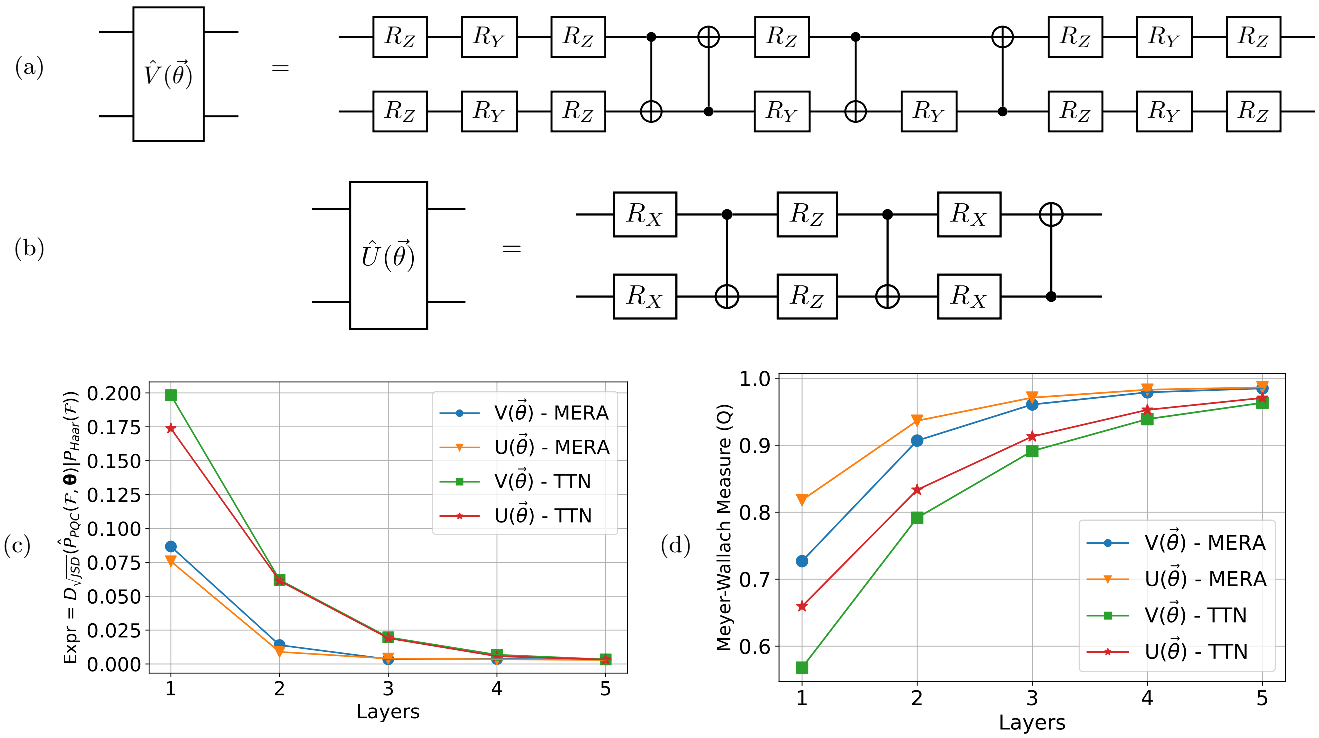

FIG. 2: **Unitary blocks and their analysis**: The possible choices of of unitary blocks for building variational ansätze are (a) $V(\vec{\theta})$, which can represent any element from $SU(4)$ group, and (b) $U(\vec{\theta})$, which is a two-qubit entangling unitary. For comparing the effectiveness of built TTN and MERA tensor network ansätze, we perform (a) expressibility analysis based on the Jensen-Shannon divergence of fidelity distributions of generated parameterized states with that of Haar states (lower the better), and (b) entangling power analysis based on the Meyer-Wallach measure (higher the better)

III. Experiments and Results

A. Circuit Architecture

We have used Tree Tensor Network (TTN) and the Multi-scale Entanglement Renormalization Ansatz (MERA) in our experiments. The TTN ansatz has a binary-tree-like structure with unitaries applied to the adjacent nodes, as shown in the Fig. 1a, which depends on the bond dimension D of the tensor network. As mentioned earlier, the bond dimension equals $D = 2^v$, where v is the number of qubits connecting the subtrees. In our case, we have used $v = 1$; therefore, our ansatz has a bond dimension two. On the other hand, the structure of the MERA tensor network can be explained using a TTN itself, where it can be constructed by adding a set of unitaries to consecutive nodes of the TTN as shown in Fig. 1b.

The choice of the unitary block $U_B(\vec{\theta})$ is a crucial one, which depends on D and results in varied performance between different ansatz structures. In our case, we compare the performance of MERA- and TTN-based ansatz built using the unitary block $\hat{V}(\vec{\theta})$ and $\hat{U}(\vec{\theta})$ based on metrics of expressibility and entangling capability defined in the qLEET library [14]. In particular, we want our ansatz to be more expressive and capable of generating entanglement. For the former, we compare the divergence using the Jensen-Shannon distance (JSD) between the fidelity distributions for the states generated by Haar Random unitaries ($P_{\mathrm{Haar}}(\mathcal{F})$) and the ansatz ($\hat{P}_{PQC}(\mathcal{F}, \vec{\theta})$). The smaller this divergence, the closer ansatz is to a Haar random unitary and hence more expressive it comes out to be. In contrast, to compare the latter, we use an entanglement measure known as the Mayer-Wallach measure, which quantifies the average entanglement in all the states produced by an ansatz by measuring the average linear entropy over all possible single-qubit subsystems.

We present the structure description of $U(\vec{\theta})$ and $V(\vec{\theta})$ in Figs. 2a and 2b. The first one is a general element of the $SU(4)$ group and comprises four controlled-NOTs and 15 single-qubits rotations. In distinction, the other is a two-qubit entangler gate comprising three controlled-NOTS and six single-qubit rotations. In the Figs. 2c and 2d, we look at expressibility and entangling capability, respectively. As a general trend we see that MERA-based ansatz is more expressible and generated more entangled states than TTN-based ansatz. Additionally, amongst $U(\vec{\theta})$ and $V(\vec{\theta})$, in both the cases, for single layered cir-

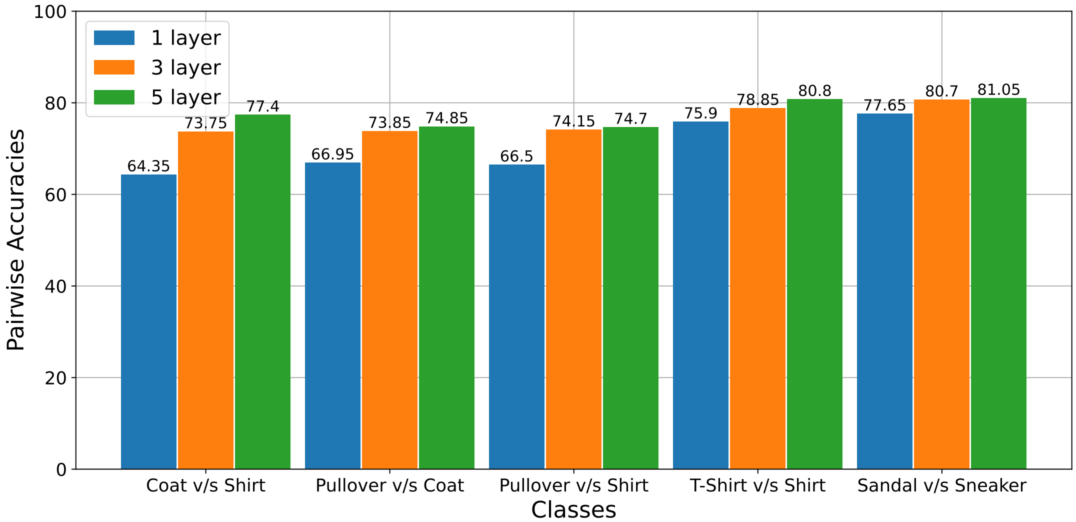

FIG. 3: Performance of the MERA tensor network ansatz with different layers

cuits ($L = 1$), the ansatz built using $U(\vec{\theta})$ comes out to be more effective than $V(\vec{\theta})$. Moreover, since the number of variational parameters are lesser in case of the $U(\vec{\theta})$ and $V(\vec{\theta})$ are in the ratio $2:5$, the former will be much more easier to be optimized and hence will be more scalable for the larger systems. Moreover, while in the case of expressibility, for multiple layers ($L > 1$), for each MERA- and TTN-based ansatz, the circuits with $U(\vec{\theta})$ and $V(\vec{\theta})$ becomes equally expressible, but the former is still able to produce more entangled states than the latter. Therefore, based on these observation we have used tensor network ansatz based on the $U_B = U(\vec{\theta})$.

B. Tasks

1. *Image Classification*

a. Dataset

We have conducted the image classification tasks on the Fashion-MNIST dataset [15]. It is a set of 28×28 gray scale images with 10 classes (tshirt, trousers, pullover etc.) with 6000 train and 1000 test samples in each class. Most of the image classification tasks done using quantum tensor networks use the MNIST dataset [30]. We have chosen the Fashion-MNIST dataset is less overused as it is more complicated than the MNIST dataset, which is essentially solved at this point [31]. Therefore obtaining better accuracies at Fashion-MNIST would better represent the effectiveness of the learning models.

b. Encoding Strategy

In order to process classical data using a quantum circuit, we first need to embed it in a quantum state. For our experiments, we have used amplitude embedding in which

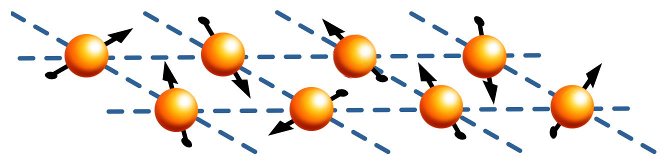

FIG. 4: 2-D lattice of eight spins in paramagnetic state

encoding an image of size $N \times M$ will require $log_2(N \times M)$ qubits. Each image of size 28×28 is first converted to a linear vector of size 1×28^2. In case the image size is too large to process, it is first resized and then transformed into the image vector. The image vector is then mapped to a state in the Hilbert Space. A variety of feature maps can be used for this purpose. So each image in the Fashion-MNIST dataset was first resized and converted to an image vector. The image vector was then normalized and encoded into the amplitudes of an eight qubit quantum state.

c. Optimization and Hyperparameters

The ADAM optimizer [32] was used to optimize the training process with a learning rate of 0.01. A mini-batch size of 20 was used and the model was trained over 40 epochs. We used the categorical cross entropy as the loss function. The measurement taken on the third qubit was used to calculate the loss along with a softmax function for pairwise accuracy calculations.

d. Results

We used eight qubit ansatz based on both TTN and MERA tensor network states. Amongst them, the latter one obtained reasonably better results for all pairs of classes of the Fashion MNIST dataset and therefore we present only its results here. Predictably, we see a better

T-shirt	-									
Trouser	0.953	-								
Pullover	0.894	0.966	-							
Dress	0.8655	0.9155	0.9615	-						
Coat	0.8315	0.944	0.6695	0.8875	-					
Sandal	0.9085	0.977	0.9745	0.9795	0.8925	-				
Shirt	0.759	0.9405	0.665	0.8935	0.6435	0.9725	-			
Sneaker	0.988	0.992	0.9925	0.993	0.995	0.7765	0.994	-		
Bag	0.9155	0.9645	0.939	0.9445	0.8975	0.7895	0.9335	0.9215	-	
Ankle boot	0.9845	0.9815	0.993	0.98	0.98	0.79	0.9845	0.8925	0.9895	-
Layer: 1	T-shirt	Trouser	Pullover	Dress	Coat	Sandal	Shirt	Sneaker	Bag	Ankle boot

TABLE I: Pairwise accuracy on the classes of the Fashion MNIST dataset for one layer of the MERA tensor network

T-shirt	-									
Trouser	0.9585	-								
Pullover	0.9375	0.974	-							
Dress	0.8805	0.9445	0.9655	-						
Coat	0.8955	0.959	0.7385	0.891	-					
Sandal	0.982	0.986	0.989	0.9915	0.98	-				
Shirt	0.7875	0.963	0.7415	0.9005	0.7375	0.9825	-			
Sneaker	0.992	0.9945	0.9955	0.9965	0.998	0.807	0.9955	-		
Bag	0.968	0.9775	0.958	0.962	0.973	0.94	0.9475	0.964	-	
Ankle boot	0.989	0.986	0.998	0.9915	0.992	0.799	0.992	0.8975	0.9915	-
Layers: 3	T-shirt	Trouser	Pullover	Dress	Coat	Sandal	Shirt	Sneaker	Bag	Ankle boot

TABLE II: Pairwise accuracy on the classes of the Fashion MNIST dataset for three layers of the MERA tensor network

T-shirt	-									
Trouser	0.959	-								
Pullover	0.939	0.9755	-							
Dress	0.8895	0.9515	0.9655	-						
Coat	0.9285	0.964	0.7485	0.8965	-					
Sandal	0.99	0.9915	0.995	0.992	0.9935	-				
Shirt	0.788	0.964	0.747	0.905	0.774	0.9865	-			
Sneaker	0.9925	0.9975	0.999	0.9975	0.9985	0.8105	0.997	-		
Bag	0.9695	0.9775	0.963	0.969	0.974	0.9425	0.955	0.9805	-	
Ankle boot	0.99	0.9885	0.9985	0.9945	0.992	0.8315	0.9965	0.898	0.994	-
Layers: 5	T-shirt	Trouser	Pullover	Dress	Coat	Sandal	Shirt	Sneaker	Bag	Ankle boot

TABLE III: Pairwise accuracy on the classes of the Fashion MNIST dataset for five layers of the MERA tensor network

performance on classes that are more unlike each other like Pullover vs Ankle boot (99.3%) than classes that are similar to each other like coat and shirt(64.35%).

Increasing the number of layers to three and five has shown an increase in the pairwise accuracy especially in our previous case of the coat and shirt labels where the accuracy increases from 64.35% to 73.75% to 77.4% as can be seen in Tables I, II and III. Such a trend is observed in most classes where one layer of the MERA or TTN ansatz did not perform very well.

We observe a bigger difference in accuracy when going from one layer to three layers than when going from three layers to five layers. In fact, in most cases, we see a similar performance in ansätz with three and five layers. Fig. 3 shows the pairwise accuracy for certain pairs of classes as the number of layers is increased, which cor-

Spin Model	Lattice	Tensor Network States	Test Accuracies	
			8 spins (on simulator)	4 spins (on IBMQ Nairobi)
Heisenberg	Line	MERA	98.6 ± 0.7	74
Heisenberg	Line	TTN	96.5 ± 1.03	72.6
Transverse Ising	Line	MERA	99.8 ± 0.06	88.2
Transverse Ising	Line	TTN	98.3 ± 0.1	84.5
Heisenberg	Square	MERA	98.5 ± 0.88	68.6
Heisenberg	Sqaure	TTN	96.3 ± 1.25	64.0
Transverse Ising	Square	MERA	99.8 ± 0.06	73.6
Transverse Ising	Square	TTN	98 ± 0.09	72.1

TABLE IV: Performance of the TTN and MERA tensor networks on recognizing correct phases of various spin systems on line and square lattices. For eight spins systems, simulations were performed numerically on a quantum simulator and results were averaged over five trials. Whereas, for the four spins systems, experiments were executed on the IBMQ Nairobi, a seven-qubit quantum hardware and the best results out of 3 trials are being reported here.

roborates the increasing trends of expressibility and entangling power in Figs. 2c and 2d.

2. *Quantum Phase Recognition*

a. Models and Data generation

1. 1-D Transverse-field Ising Model

The Transverse-field Ising Model in 1 dimension is characterized by the Hamiltonian:

$$\hat{H}(h) = J\sum_{i=1}^{n} \hat{\sigma}_i^z \hat{\sigma}_{i+1}^z + h\sum_{i=1}^{n} \hat{\sigma}_i^x$$

Where J is the coupling constant, h the external magnetic field and σ_i^z and σ_i^x are the Pauli matrices Z and X acting on the i^{th} spin. We have taken $J = 1$ in our experiments. When $h < 1$, the nearest neighbor term dominates. This leads to the spins aligning in either an up or down direction. This results in a disordered paramagnetic phase. For $h > 1$, the 2^{nd} term dominates. The spins end up aligning themselves with the external magnetic field leading to an ordered ferromagnetic phase. A phase transition occurs at $h = J$ [29].

In our experiments, we have generated 1000 ground states for line systems with four and eight spins using the given Hamiltonian with $J = 1$ and h varying from 0 to $2J$.

2. 1-D XXZ Heisenberg Model

The energy of the 1-D XXZ Heisenberg Model is described using the Hamiltonian:

$$\hat{H}(h) = J\sum_{i=1}^{n} \hat{\sigma}_i^x \hat{\sigma}_{i+1}^x + \hat{\sigma}_i^y \hat{\sigma}_{i+1}^y + \Delta \hat{\sigma}_i^z \hat{\sigma}_{i+1}^z$$

Where J is again the coupling constant and taken as 1 in our experiments. Δ introduces anisotropy in the interaction in the z axis. It is observed that for $\Delta \to \infty$, the system is in the antiferromagnetic/ Néel state i.e all neighboring spins are alternating i.e spin up or down. As Δ approaches 1, the system changes such that all the spins are now in the $x-y$ plane for $\Delta < 1$. The system in this case is in a paramagnetic phase [27]. As Δ reduces further, for $\Delta < -1$, all the spins arrange themselves in the same direction resulting in a ferromagnetic phase. Clearly, for $J = 1$, a phase change occurs at $\Delta = 1$ and -1 [27, 33].

The data for the 1-D XXZ Heisenberg Model was generated for line systems with four and eight spins using the given Hamiltonian with $J = 1$ and Δ varying from -2 to 2 for a 1000 points.

3. 2-D Transverse-field Ising Model

The 2-D Transverse-field Ising model has the same Hamiltonian as the 1-D case. However, a phase transition is observed at $h \approx 3J$ [34]. The data is generated for a 1000 points for a 2-D lattice of four and eight spins (2×4) using the given Hamiltonian with $J = 1$ and h varying from 0 to $6J$. The phase transition is seen at $h = 3J$. Fig. 4 shows a 2-D lattice of spin systems.

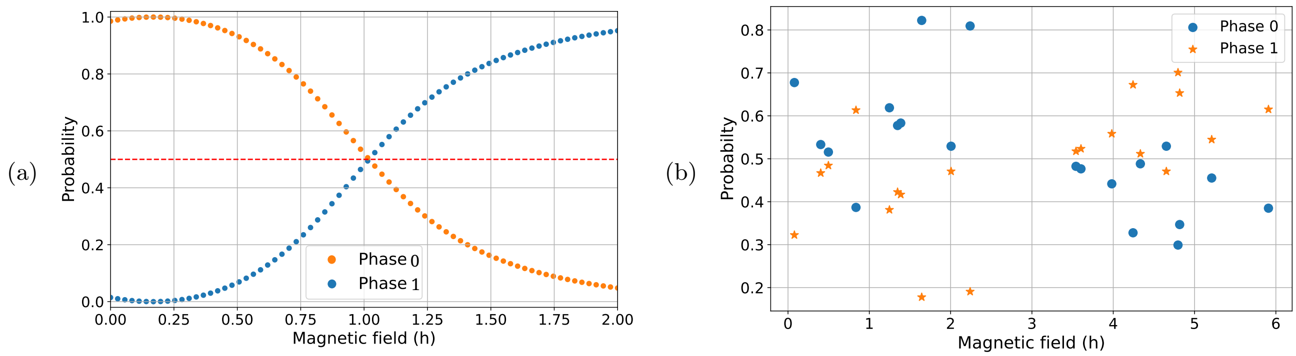

FIG. 5: **Prediction probabilities of phases with MERA based ansatz**: (a) for transverse-field Ising model in 1-D case (noiseless simulation), and (b) For transverse-field Ising model in 2-D case (executed on IBMQ Nairobi, a 7-qubit hardware)

4. 2-D XXZ Heisenberg Model

The 2-D XXZ Heisenberg Model has the same Hamiltonian as the 1-D case with a phase transition occurring at $\Delta = 1$ and -1 as well [35]. The data generation process is the exact same as that in the 1-D case.

b. Training

The circuit was training using the variational quantum algorithm as shown in Fig 1b. The data was split randomly into train, validation and test sets in the ratio $3 : 1 : 1$. Measurements were taken on the third and sixth qubits and cross entropy loss was calculated. A batch size of 8 was used with a learning rate of 0.002 for the MERA ansatz and 0.0008 for the TTN ansatz. The ADAM optimizer [32] was used to optimize the training process over 2000 iterations.

c. Results

We see that both the MERA and the Tree tensor network perform well on the Heisenberg and the Transverse Ising models in both 1-D and 2-D. The MERA tensor network gives slightly better results as compared to the tree tensor network. The networks perform better on the Transverse Ising model overall than the Heisenberg model (Table IV). Moreover, the performance of both the tensor networks on the 1-D case is better than the more complicated 2-D case. Fig. 5a shows the results outputted by our model. When the probability of a phase is more than 50% we assign our output the label corresponding that phase. We see that our model is more confident when the value of h is further from the point of phase transition i.e. when h is 1. Fig. 5b shows the values our model outputs when the models were trained and executed on the IBMQ Nairobi, which is their 7-qubit superconducting quantum hardware.

IV. Conclusions

In this paper, we have studied the performance of quantum tensor networks for image classification tasks and quantum phase recognition tasks of spin systems.

We have extended the previous works done in this domain in the following two ways. First, we have presented a strategy based on metrics like expressibility, and entangling capability of the parameterized circuits to choose a well-suited block structure for the tensor-network inspired ansäatze. Such analysis was corroborated by the results obtained for the task of image classification, where we were able to increase the performance of our classifiers by increasing the number of layers of the circuits. Second, for the quantum phase recognition task, we have attempted to study spin systems on 2-D lattices with the tensor-network ansatz, which are generally more challenging than those on 1-D spin lattices that have been studied in the literature until now [16, 26].

In the image classification task, the pairwise accuracies between the different classes of the Fashion-MNIST dataset were calculated for 1, 3, and 5 layers of the MERA tensor network ansatz. The results are shown in Tables I, II and III. We see a clear increase in accuracy when the number of layers is increased, especially when we go from a single layer to three layers. The performance of the ansatz with five layers is slightly more than when three layers are used. This is corroborated by Fig. 2c, where we see a marked increase in the expressibility of our circuit when the number of layers is increased from one to three but not a lot of increase when going from three layers to five. In pairs of classes where one layer of the ansatz performed poorly, like coat vs. shirt or sandals vs. sneakers, we see an appreciable increase in accuracy with an increase in layers. Possibly, this happens because the layered structure allows correlation to be distributed more effectively among the qubits allowing the system to evolve to the states that were not previously possible. More explicitly, ansatz becomes more expressible with each layer, and its entangling power also gets enhanced.

This can be easily seen in the results we obtain for the entangling power analysis as shown in Fig. 2d, where entanglement measures for both TTN and MERA follow a similar exponential trend of improvement with each layer before plateauing down.

In the quantum phase recognition tasks, we first use a VQE-based variational routine with a hardware efficient ansatz to prepare these systems in the ground state of the Hamiltonian for each spin system instance. This enables us to take care of the sign problem by employing the hybrid quantum-classical routine. Furthermore, the TTN and MERA tensor network ansatz results indicate their effectiveness at solving many-body physics problems. However, among the two, we find that MERA is superior in performance for such tasks than TTN, possibly due to being more expressible and generating more entanglement in the states it evolves. In addition to this, we also see that it was much easier for tensor-network-based ansatz to work for the Transverse Ising model, which has simpler interaction terms than the XXZ Heisenberg models. This is in agreement with the previous results for these two models [26]. Moreover, even for a given model, we see that results for linear 1-D systems were better than those for the system on 2-D lattices. This is again due to fewer interacting terms, as seen in the previous observation. Finally, we also executed our classifiers on the actual quantum hardware, IBMQ Nairobi, for classifying phases of four spin systems for both 1-D and 2-D cases. We see that even though there's a decreased performance due to the noise present on the device, it was still able to classify the phases decently (Fig. 5b). We speculate that this performance can be further improved by employing specific error mitigation techniques like those available in Mitiq [36].

Overall, our studies have shown promising results in both tasks, and we conclude that tensor-network-inspired ansatz is an ideal candidate for quantum-enhanced learning of both quantum and classical data. For quantum data, further studies need to be done on tasks such as the phase recognition task on larger, more complicated systems, like systems with 16 or 24 spins, to see how scalable our current model is, which is something we are currently pursuing. On the other hand, for the classical data, more specifically, for the image classification tasks, more work is required to study higher resolution images that would require much better encoding strategies, which is another area of our interest.

Data Availability

The code created to run the presented simulations and any related supplementary data could be made available to any reader upon reasonable request.

Acknowledgements

We acknowledge the use of IBM Quantum services for this work. The views expressed are those of the authors, and do not reflect the official policy or position of IBM or the IBM Quantum team.

[1] L. Deng and X. Li, *Machine Learning Paradigms for Speech Recognition: An Overview*, IEEE Transactions on Audio, Speech, and Language Processing **21**, 1060 (2013).

[2] A. Popli, S. Tandon, J. J. Engelsma, N. Onoe, A. Okubo, and A. Namboodiri, A Unified Model for Fingerprint Authentication and Presentation Attack Detection (2021).

[3] D. C. Cireşan, U. Meier, J. Masci, L. M. Gambardella, and J. Schmidhuber, *High-Performance Neural Networks for Visual Object Classification*, arXiv e-prints (2011), arXiv:1102.0183 [cs.AI].

[4] M. Amrane, S. Oukid, I. Gagaoua, and T. Ensari, in *2018 Electric Electronics, Computer Science, Biomedical Engineerings' Meeting (EBBT)* (IEEE, 2018).

[5] J. Carrasquilla and R. G. Melko, *Machine learning phases of matter*, Nature Physics **13**, 431 (2017).

[6] E. P. L. van Nieuwenburg, Y.-H. Liu, and S. D. Huber, *Learning phase transitions by confusion*, Nature Physics **13**, 435 (2017).

[7] X. Zhang, G. Pan, X. Y. Xu, and Z. Y. Meng, *Sign Problem Finds Its Bounds*, arXiv e-prints (2021), arXiv:2112.06139 [cond-mat.str-el].

[8] E. Farhi and H. Neven, Classification with Quantum Neural Networks on Near Term Processors (2018).

[9] A. Peruzzo, J. McClean, P. Shadbolt, M.-H. Yung, X.-Q. Zhou, P. J. Love, A. Aspuru-Guzik, and J. L. O'Brien, *A variational eigenvalue solver on a photonic quantum processor*, Nature Communications **5**, 10.1038/ncomms5213 (2014).

[10] C. Bravo-Prieto, R. LaRose, M. Cerezo, Y. Subasi, L. Cincio, and P. J. Coles, *Variational Quantum Linear Solver*, arXiv e-prints (2019), arXiv:1909.05820 [quant-ph].

[11] J. Preskill, *Quantum Computing in the NISQ era and beyond*, Quantum **2**, 79 (2018).

[12] M. Cerezo, A. Arrasmith, R. Babbush, S. C. Benjamin, S. Endo, K. Fujii, J. R. McClean, K. Mitarai, X. Yuan, L. Cincio, and P. J. Coles, *Variational Quantum Algorithms*, arXiv e-prints (2020), arXiv:2012.09265 [quant-ph].

[13] U. Azad and H. Singh, *Quantum chemistry calculations using energy derivatives on quantum computers*, Chemical Physics **558**, 111506 (2022).

[14] U. Azad and A. Sinha, *qLEET: Visualizing Loss Landscapes, Expressibility, Entangling Power and Training Trajectories for Parameterized Quantum Circuits*, arXiv e-prints (2022), arXiv:2205.02095 [quant-ph].

[15] H. Xiao, K. Rasul, and R. Vollgraf, Fashion-MNIST: a Novel Image Dataset for Benchmarking Machine Learn-

ing Algorithms (2017).

[16] M. Lazzarin, D. E. Galli, and E. Prati, *Multi-class quantum classifiers with tensor network circuits for quantum phase recognition*, Physics Letters A **434**, 128056 (2022).

[17] E. Stoudenmire and D. J. Schwab, in *Advances in Neural Information Processing Systems*, Vol. 29, edited by D. Lee, M. Sugiyama, U. Luxburg, I. Guyon, and R. Garnett (Curran Associates, Inc., 2016).

[18] R. Orús, *A practical introduction to tensor networks: Matrix product states and projected entangled pair states*, Annals of Physics **349**, 117 (2014).

[19] Y.-Y. Shi, L.-M. Duan, and G. Vidal, *Classical simulation of quantum many-body systems with a tree tensor network*, Physical Review A **74**, 10.1103/physreva.74.022320 (2006).

[20] G. Vidal, *Class of Quantum Many-Body States That Can Be Efficiently Simulated*, Phys. Rev. Lett. **101**, 110501 (2008).

[21] W. Huggins, P. Patil, B. Mitchell, K. B. Whaley, and E. M. Stoudenmire, *Towards quantum machine learning with tensor networks*, Quantum Science and Technology **4**, 024001 (2019).

[22] R. Haghshenas, J. Gray, A. C. Potter, and G. K.-L. Chan, *Variational Power of Quantum Circuit Tensor Networks*, Physical Review X **12**, 10.1103/physrevx.12.011047 (2022).

[23] M. L. Wall, M. R. Abernathy, and G. Quiroz, *Generative machine learning with tensor networks: Benchmarks on near-term quantum computers*, Physical Review Research **3**, 10.1103/physrevresearch.3.023010 (2021).

[24] E. Grant, M. Benedetti, S. Cao, A. Hallam, J. Lockhart, V. Stojevic, A. G. Green, and S. Severini, *Hierarchical quantum classifiers*, npj Quantum Information **4**, 10.1038/s41534-018-0116-9 (2018).

[25] S. Yen-Chi Chen, C.-M. Huang, C.-W. Hsing, and Y.-J. Kao, *Hybrid quantum-classical classifier based on tensor network and variational quantum circuit*, arXiv e-prints (2020), arXiv:2011.14651.

[26] A. V. Uvarov, A. S. Kardashin, and J. D. Biamonte, *Machine learning phase transitions with a quantum processor*, Phys. Rev. A **102**, 012415 (2020).

[27] J. Parkinson and D. J. J. Farnell, *An Introduction to Quantum Spin Systems* (Springer Berlin Heidelberg, 2010).

[28] V. Ohanyan, Introduction to quantum spin chains, lecture notes (2015).

[29] A. Tan, Quantum Ising Models (2018).

[30] Y. LeCun and C. Cortes, MNIST handwritten digit database (2012).

[31] Z. SE, Fashion MNIST Benchmark (2017).

[32] D. P. Kingma and J. Ba, *Adam: A Method for Stochastic Optimization*, arXiv e-prints , arXiv:1412.6980 (2014), arXiv:1412.6980 [cs.LG].

[33] F. Franchini, *An Introduction to Integrable Techniques for One-Dimensional Quantum Systems* (Springer International Publishing, 2017).

[34] T. Hashizume, I. P. McCulloch, and J. C. Halimeh, *Dynamical phase transitions in the two-dimensional transverse-field Ising model*, Physical Review Research **4**, 10.1103/physrevresearch.4.013250 (2022).

[35] O. S. Sarıyer, *Two-dimensional quantum-spin-1/2 XXZ magnet in zero magnetic field: Global thermodynamics from renormalisation group theory*, Philosophical Magazine **99**, 1787 (2019).

[36] R. LaRose, A. Mari, S. Kaiser, P. J. Karalekas, A. A. Alves, P. Czarnik, M. El Mandouh, M. H. Gordon, Y. Hindy, A. Robertson, P. Thakre, N. Shammah, and W. J. Zeng, *Mitiq: A software package for error mitigation on noisy quantum computers*, arXiv e-prints , arXiv:2009.04417 (2020), arXiv:2009.04417 [quant-ph].